Toxicology Research

Accepted Manuscript

ROYAL SOCIETY OF CHEMISTRY

www.rsc.org/toxicology

Journal Name Toxicology Research Dynamic Article Links ►

Cite this: DOI: 10.1039/c0xx00000x

www.rsc.org/xxxxxx

FULL PAPER

Kinetic and Density Functional Theory (DFT) Studies of *in vitro* Reactions of Acrylamide with the Thiols: Captopril, *L*-Cysteine, and Glutathione

Grace-Anne Bent*[a], Paul Maragh[b], Tara Dasgupta[b], Richard A. Fairman[a], and Lebert Grierson[a]

Received (in XXX, XXX) Xth XXXXXXXXX 20XX, Accepted Xth XXXXXXXXX 20XX
DOI: 10.1039/b000000x

The kinetics for the *in vitro* reactions of acrylamide (AA), a potentially toxic food contaminant formed during high-temperature food preparation, with captopril (CapSH), *L*-cysteine (CySH) and glutathione (GSH) were determined under basic conditions and constant ionic strength (pH 7.10 – 9.10; I = 0.2 mol dm^{-3}, NaCl), and pseudo first-order conditions with respect to AA. The second-order rate constants, *k,* and activation parameters ($\Delta H^{\ddagger}$, $\Delta S^{\ddagger}$, and $\Delta G^{\ddagger}$) were determined over the ranges of $293 \leq \theta \geq 303$ K for CySH and $303 \leq \theta \geq 315$ K for GSH and CapSH. Comparison of experimental second-order rate constants at 303 K for CapSH, CySH, and GSH were: 0.13 ± 0.01, 0.34 ± 0.02, and 0.18 ± 0.02 dm^3 mol^{-1} s^{-1}, respectively and DFT calculations show evidence of diminished intra-molecular hydrogen abstraction reaction in aqueous solution specific only to GSH. An isokinetic plot of $\Delta H^{\ddagger}$ versus $\Delta S^{\ddagger}$ yields an isokinetic temperature of 260 ± 24 K and an intercept, $\Delta G^{\ddagger}$, of 71 ± 4 kJ mol^{-1} indicating that AA reacts with all three thiols via the similar reaction mechanism. Theoretically determined $\Delta G^{\ddagger}$ values in aqueous solution (DFT-BVP86/Ahlrichs-TZVP/COSMO-RS) for CapSH, CySH, and GSH, including their zero point vibrational energy, are 212.2, 217.8, and 253.4 kJ mol^{-1}, respectively at 298 K.

KEYWORDS: acrylamide, *L*-cysteine, glutathione, captopril, reaction kinetics, isokinetic plot, minimum energy path density functional calculation

Introduction

Acrylamide (AA), a known neurotoxin and potential human carcinogen [1-4] was recently discovered in foods [5]. Research is currently underway to quantify the levels of AA in various foods [6, 7]. Limited data is available on AA's interaction within biological systems and as such studies (*in vivo* and *in vitro*) are being conducted to assess the potential of AA toxicity and carcinogenicity [8]. *α,β*-unsaturated carbonyl compounds such as AA react readily with thiolate anions (RS^-) by Michael addition and have been widely used to selectively modify thiol groups of structural and functional proteins [9]. Friedman [10] has reported on the use of AA to alkylate the thiol groups of various enzymes. However, the relationship of such reactions to AA's toxicity and potential carcinogenicity is unknown. Kinetically, the Michael additional reaction scheme of thiols with AA is shown below:

$$RSH \underset{k}{\overset{K_s}{\rightleftharpoons}} RS^- + H^+ \qquad (1)$$

$$RS^- + H_2C{=}CHCONH_2 + H_2O \longrightarrow RS{-}CH_2CH_2CONH_2 + OH^- \qquad (2)$$

Tong et al. [9] reported on the reactions of AA with glutathione (GSH) and human serum albumin (HSA), two of the most abundant thiols within the human body. The rate constants, with phosphate buffer, were found to be 0.021 dm^3 mol^{-1} s^{-1} and 0.0054 dm^3 mol^{-1} s^{-1}, respectively under physiological conditions. The reaction was conducted under pseudo-first order conditions with AA in large excess. The amount of unreacted thiol was determined by withdrawing portions of the reaction mixture at various times and reacting with Ellman's reagent, 5,5'-dithiobis(2-nitrobenzoic acid), commonly symbolized as ESSE. The residual Ellman's thiolate anion (ES^-) was monitored spectrophotometrically following the Ellman's scheme [11].

L-Cysteine (CySH) and (GSH) are important thiols synthesised within the body. They form part of the body's natural defence mechanism [12, 13] by scavenging free radicals and helping to maintain the secondary structure of certain proteins [14, 15]. Captopril (CapSH) is also important as a vasodilator in the treatment of congestive heart failure where it protects NO from oxidation by scavenging free oxygen radicals [16-19].

In this report, the reactions of AA with CapSH, CySH and GSH were investigated with a Tris/HCl buffer system by monitoring the rate of disappearance of ES^- at 409 nm. We present a comprehensive study on the reaction rates of CapSH with AA, including theoretical investigation of the minimum energy pathway for the reaction by density functional theory (DFT). How AA reacts with these thiols, thus reducing or enhancing their ability to carry out their function within the body, is of great importance in understanding the mechanism and metabolism of AA.

Materials and Methods

Chemicals

Acrylamide (electrophoresis grade), AR grade captopril, *L*-cysteine, glutathione, Ellman's reagent, (ESSE), sodium chloride, Tris.HCl, potassium hydrogen phthalate, potassium dihydrogen phosphate, ascorbic acid (H_2ASc), and HPLC grade methanol were purchased from Aldrich (Fairlawn, NJ). Deionised water was prepared in house using a Labconco Water Pro PS deionizer (Labconco Water Corporation, Kansas City, MO). All stock and working solutions were prepared in deionised water. HCl (Analar grade) was obtained from BDH Laboratories (Poole, England).

Spectrophotometric Measurements

The acrylamide-thiolate (AA-SR) complexes were monitored spectrophotometrically on a HP 8453 Diode Array Spectrophotometer with 1 cm path length quartz cuvettes. The wavelengths monitored were 327 nm for ESSE and 409 nm for the Ellman's thiolate (ES^-) anion. The diode array spectrophotometer was operated in the kinetic mode for determination of reaction parameters and in the standard mode for quantifying the rate constants associated with each AA-thiol reaction. Temperature was maintained by a Lauda-Brinkmann RM6 B Ciculator/Thermostated Water Bath (Lauda Dr. R. Wobser, GMBH and Co., Lauda-Königshofen, Germany).

In the kinetic mode, all reactions were conducted at 310 K. In the standard mode with varied AA concentrations, the reactions were conducted at 310 K. For varied thiol concentrations, the reactions were conducted at 293, 298, 303 K for CySH and 303, 310, and 315 K for CapSH and GSH. Mixtures containing CapSH and GSH were measured at 1 minute intervals while CySH mixtures were measured at 30 s intervals. The pH of the final solutions were recorded using an Orion Research Expandable ion Analyzer EA 920 (Orion Research Inc., Boston, M.A., U.S.A.) calibrated with buffers: 4.01 (0.0496 mol dm^{-3} $K_2HC_8H_4O_4$) and 6.87 (0.025 mol dm^{-3} KH_2PO_4).

LC/DAD/MS Analysis

The AA–SR complexes were analyzed on an Agilent 1100 Series LC coupled to an Agilent 1100 Series MS Detector (Agilent, Technologies, Palo Alto, CA, U.S.A.). Separation of the complexes were achieved using a Zorbax Eclipse XDB–C18 column (150 mm x 4.6 mm ID x 5 µm particle size; Agilent Technologies, Palo Alto, CA, U.S.A.) with a Zorbax XDB–C18 guard column (12.5 mm x 4.6 mm i.d.) at a flow rate of 0.2 mL/min; Operating parameters were: positive electrospray ionization (+ESI) in the SIM and scan modes; SIM ions: 308, 379, 380, 613; scan range: 300 – 400 amu (for the AA–SG complex); Mobile phase: methanol/water (5 + 95 v/v)%; run time 8.00 min; MS: Drying gas temperature: 350 ^oC; drying gas flow: 12 L/min; nebulizer gas pressure: 35 psig; capillary voltage: 3000 V.; Fragmentor voltage: 80V (scan), 70V (SIM); DAD: 195 ± 10 nm with a reference of 360 ± 100 nm.

Preparation of Thiol Solutions

Preliminary Studies

Stability of Thiols

Solutions of CapSH, CySH, and GSH, were all prepared at concentrations of 6.5 x 10^{-4} mol dm^{-3} in deionised water. 1.00 mL of each thiol solution was transferred to 10.00 mL volumetric flasks containing Tris/HCl buffer solutions (pH 7.4; ionic strength (I) = 0.2 mol dm^{-3} (NaCl)) or HCl (pH 4.5; I = 0.2 mol dm^{-3} (NaCl)) and made up to the mark with deionised water for a final thiol concentration of 6.5 x 10^{-5} mol dm^{-3}.

A 1.0 x 10^{-4} mol dm^{-3} stock solution of ESSE was prepared in deionised water. 1.00 mL of each of the buffered thiol solutions and 1.00 mL of ESSE were mixed in 1 cm quartz cuvettes. The reactions were monitored spectrophotometically in the kinetic mode at 310 K at a cycle time of 10 s for 9000 s.

Variation of Acrylamide Concentration

1.00 mL of each thiol solution was transferred to 10.00 mL volumetric flasks containing Tris/HCl buffer solutions (pH 7.4; I = 0.2 mol dm^{-3} (NaCl)). A 1.0 mol dm^{-3} AA solution was prepared in deionised water and various amounts added to the buffer solutions for final AA concentrations ranging from 9.963 x 10^{-3} mol dm^{-3} to 9.963 x 10^{-2} mol dm^{-3} i.e. pseudo-first order conditions with respect to AA. 1.00 mL of each of the thiol buffer solutions and 1.00 mL of 1.0 x 10^{-4} mol dm^{-3} ESSE were added to quartz cuvettes at various times to measure the rate of thiol decomposition.

Variation of Thiol Concentration

Varying volumes of each thiol stock solution were added to 10.00 mL volumetric flasks containing Tris/HCl buffer solutions (pH 7.4; I = 0.2 mol dm^{-3} (NaCl)) to give final thiol concentrations within the range of 1.0 x 10^{-5} mol dm^{-3} to 1.0 x 10^{-4} mol dm^{-3}. The AA concentration was kept constant for each thiol. The AA concentration used for CapSH was 4.986 x 10^{-2} mol dm^{-3} and 9.963 x 10^{-3} mol dm^{-3} for both CySH and GSH. 1.00 mL of each of the thiol solutions and 1.00 mL of ESSE solution were added to quartz cuvettes at 30 s and 1 min intervals as described in **Spectrophotometric Measurements**. The reactions were monitored in the standard mode at a temperature at 310 K and the pseudo-first order rate constants, k_{obs}, for the thiol decomposition were calculated.

Variable Temperature Studies

Values of k_{obs}, for each thiol were determined at three temperatures while varying the pH of the mixtures. The pH range used was 7.10 – 9.10 (Tris/HCl buffer). The ionic strength was kept constant at 0.2 mol dm^{-3} (NaCl). Thiol concentration was kept at 6.5 x 10^{-5} mol dm^{-3}, and the AA concentration was also kept constant for each thiol.

The AA concentration used for CapSH, CySH, and GSH were: 4.986 x 10^{-2} mol dm^{-3}, 9.963 x 10^{-3} mol dm^{-3}, and 1.993 x 10^{-2} mol dm^{-3}, respectively. GSH and CapSH solutions were monitored at 303, 310, and 315 K while CySH solutions were monitored at 293, 298, and 303 K.

Statistical Analysis of Data

The pseudo-first order rate constants, k_{obs}, for the thiol decomposition were calculated from absorbance time data using the StatGraphics Centurion XV.I Software (SGS). k_{obs} values at each temperature were used to calculate the specific rate constants, k, and the pK_s for each thiol. Activation parameters, $\Delta H^{\ddagger}$, $\Delta S^{\ddagger}$, $\Delta G^{\ddagger}$ for each thiol were calculated from Eyring plots. Parameters generated from the Eyring plots were used to construct an isokinetic plot.

Computational Studies

Gas phase (1 atm) geometries and energies were optimized using the BVP86 DFT functional [20] and Ahlrichs' TZVP basis set [21] as available in the PQS programme [22]. Transition state geometries were optimized until a single imaginary vibrational frequency corresponding to displacement along the intrinsic reaction coordinate was found. The energy differences between reactants, transition states and products were computed relative to that of the combined energy of the isolated reactants in each case. Energy partition function analysis was used to determine the thermal corrections to the energy of each molecule (enthalpic and entropic) at different temperatures from translational, rotational and vibrational modes. With water as solvent, energies and optimized geometries were computed using the COSMO [23] electrostatic screening model and the output transferred to the ADF [24] programme for COSMO-RS [25] calculations at infinite dilution and computing the atomic charges with the Hirshfeld Atom In Molecule (AIM) method [26, 27].

Results and Discussion

The rate of disappearance of the Ellman's thiolate (ES^-) species at 409 nm is equivalent to the rate of reaction between AA and RS^-. As time progressed, more RS^- reacted with AA to form the AA–SR complex, so less RS^- was available to react with ESSE (species at 327 nm) to generate ES^-. Eventually all the RS^- was consumed and no more ES^- was formed.

Preliminary work in this study involved analysis of the reaction with AA and RSH under acidic conditions (pH 4.2 (HCl); I = 0.2 mol dm^{-3} (NaCl)), where no visible reaction was observed, supporting the reaction steps shown in equations (1) and (2); RS^- is the reactive species that reacts with AA. At 310 K, variation of AA and thiol concentrations gives a linear increase in rate at constant thiol concentration; i.e. the rate remained unchanged when the AA concentration is unchanged. This indicates that the reaction is first order with respect to AA. The pseudo-first order rate constant, k_{obs}, for each reaction is calculated according to equation (3);

$$A_t = A_\infty + (A_o - A_\infty)e^{-kt} \quad (3)$$

where: A_o is the initial absorbance; A_t is the absorbance at time t; k is the pseudo-first order rate constant.

Based on observations of increased k_{obs} with increasing pH, (**Table 1**), and the proposed reaction mechanism depicted in equations (1) and (2), the rate law (equation 4) was derived:

Table 1: Pseudo-first order rate constants for the reaction between AA and CapSH, CySH, and GSH at 303 K: pH dependence. [RSH] = 6.5 x 10^{-5} mol dm^{-3}, I = 0.2 mol dm^{-3} (NaCl), λ = 409 nm. [H_2Asc] = 1 mM for CySH

CapSH		CySH		GSH	
[AA] = 4.986 x 10^{-2} mol dm^{-3}		[AA] = 9.963 x 10^{-3} mol dm^{-3}		[AA] = 1.993 x 10^{-2} mol dm^{-3}	
pH	k_{obs} (10^{-3} s^{-1})	pH	k_{obs} (10^{-3} s^{-1})	pH	k_{obs} (10^{-3} s^{-1})
7.07	0.123	7.33	1.44	7.33	0.329
7.33	0.182	7.42	2.13	7.57	0.394
7.78	0.373	7.80	2.40	7.89	0.672
7.91	0.463	7.96	2.72	8.14	0.964
8.13	0.693	8.19	3.06	8.50	1.73
8.48	1.32	8.55	3.11	8.78	2.29
9.11	3.46	9.09	3.25	9.09	3.58

$$rate = \frac{kK_S[AA]}{K_S + [H^+]}[RSH]_{total} \quad (4)$$

which can be simplified to equation (5):

$$rate = k_{obs}\,[RSH]_{total}, \quad (5)$$

where k_{obs} is given by: $$k_{obs} = \frac{kK_S[AA]}{K_S + [H^+]} \quad (6)$$

Values for k and K_s are obtained from equation (6) using non-linear regression analysis. The pK_s for each thiol was determined from the analysis of the kinetic data. The activation parameters: $\Delta H^{‡}$ (enthalpy of activation) and $\Delta S^{‡}$ (entropy of activation), for the reaction between AA and the various thiols (RSH) were obtained from the values of the specific rate constants obtained at different temperatures using the Eyring equation:

$$R\ln\left(\frac{kh}{k_B T}\right) = -\frac{\Delta H^{\neq}}{T} + \Delta S^{\neq} \quad (7)$$

where T is temperature in Kelvin, k_B is Boltzman's constant, h is Planck's constant, and R is the standard molar gas constant.

A plot of $R\ln\left(\frac{kh}{k_B T}\right)$ versus 1/T yields a slope of $-\Delta H^{‡}$ and an intercept of $\Delta S^{‡}$. The Gibbs free energy of activation, $\Delta G^{‡}$, (at 298 K) is calculated from equation (8):

$$\Delta G^{‡} = \Delta H^{‡} - T\Delta S^{‡} \quad (8)$$

Reaction of Acrylamide and Glutathione

The repetitive-scan spectra and time trace (inset) for the reaction between AA and GSH is shown in **Figure 1**. Data for the reaction between GSH and AA with varying [GSH] are shown in **Table 2**. The plot of k_{obs} vs [AA] shows a zero intercept (**Figure 2**). **Table 2** and **Figure 2** show that k_{obs} remains unchanged when the [GSH] was varied and increased when the AA concentration increased, indicating that the reaction was pseudo-first order with respect to AA.

Cite this: DOI: 10.1039/c0xx00000x

www.rsc.org/xxxxxx

FULL PAPER

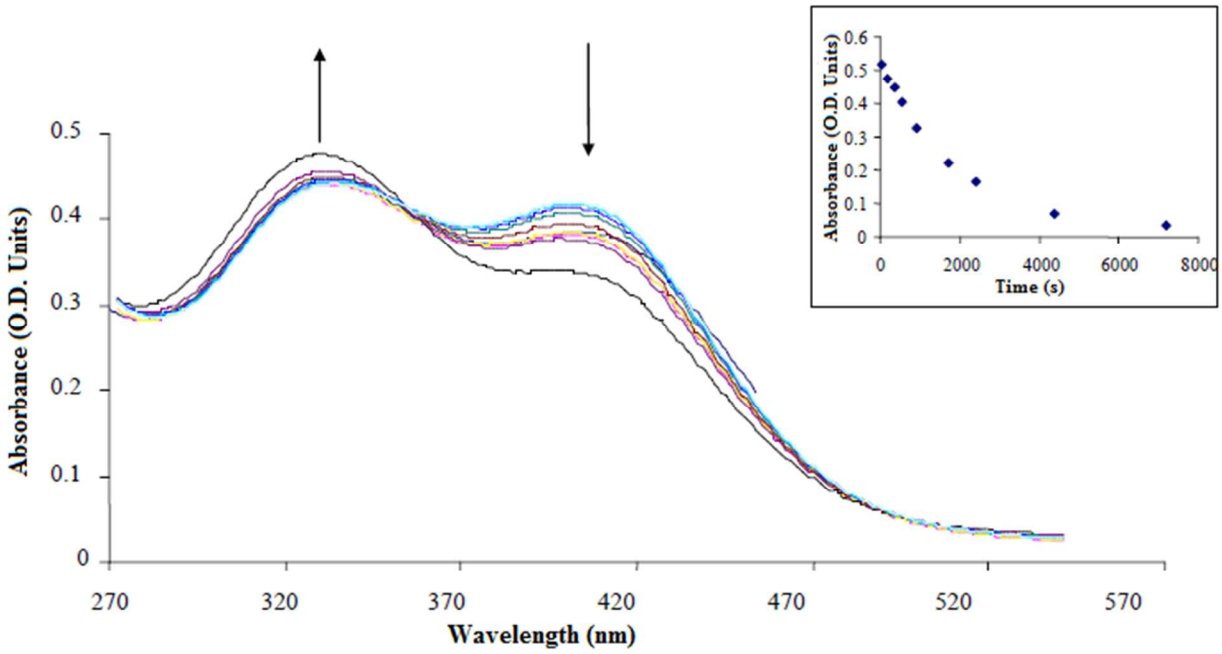

Figure 1: Repetitive-scan spectra of the reaction between AA and GSH (Inset: Absorbance-time trace showing the rate of disappearance of the ES^- species).

Table 2: Independence of k_{obs} with varying [GSH] in excess AA at 310 K; pH 7.4; [AA] = 9.963 x 10^{-2} mol dm^{-3}

[GSH] (10^{-5} mol dm^{-3})	k_{obs} (10^{-3} s^{-1})
0.863	1.1
1.29	1.1
3.47	1.3
6.93	1.0
Average and std. dev.	1.1 ± 0.1

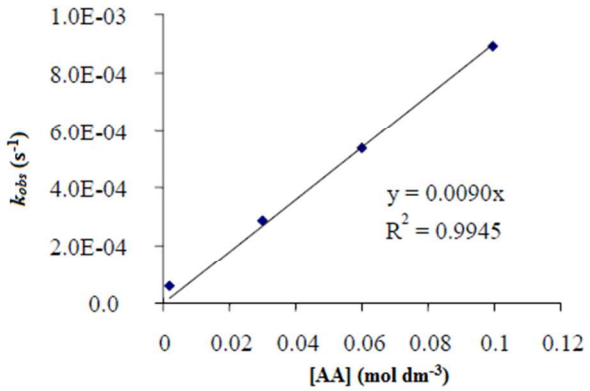

Figure 2: Pseudo-first order rate constants for the reaction of the thiolate group of GSH with varying AA at 310 K; pH 7.4; [GSH] = 6.5 x 10^{-5} mol dm^{-3}

The calculated second order rate constant for the reaction of AA with GSH at 310 K is 0.25 ± 0.01 dm^3 mol^{-1} s^{-1}, which is 10 times faster than that reported by Tong et al. [9] This could be explained by potential interaction of the phosphate buffer system that was used by Tong et al. Similar buffer interactions were absent in the Tris/HCl buffer reaction system. Hence Tris/HCl buffer was used instead of phosphate buffer system in this work. A zero intercept for the plot of k_{obs} vs [AA] (**Figure 2)** implies that the reaction of AA with the thiol group of GSH far exceeds the rate of oxidation of GSH by oxygen in air to form the disulphide, GS–SG. This was confirmed by LC/DAD/MS with +ESI operated in the SIM and scan modes (**Figure 3**). The chromatogram shows two peaks at 2.808 min and 3.170 min which correspond to GSH (unreacted) and the AA–SG adduct, respectively. The ion fragment, 308 is due to the cleavage of the AA–SG bond and subsequent reformation of GSH which picks up an additional hydrogen to become $(GSH + H)^+$. The ion fragment, 379 confirms the formation of the AA–SG species. The absence of a peak and ion fragments corresponding to the disulphide, GS–SG support our findings that the Michael addition reaction between AA and GSH occurs much faster than the oxidation of GSH by oxygen in air which results in the formation of the disulphide, GS–SG.

Cite this: DOI: 10.1039/c0xx00000x

www.rsc.org/xxxxxx

FULL PAPER

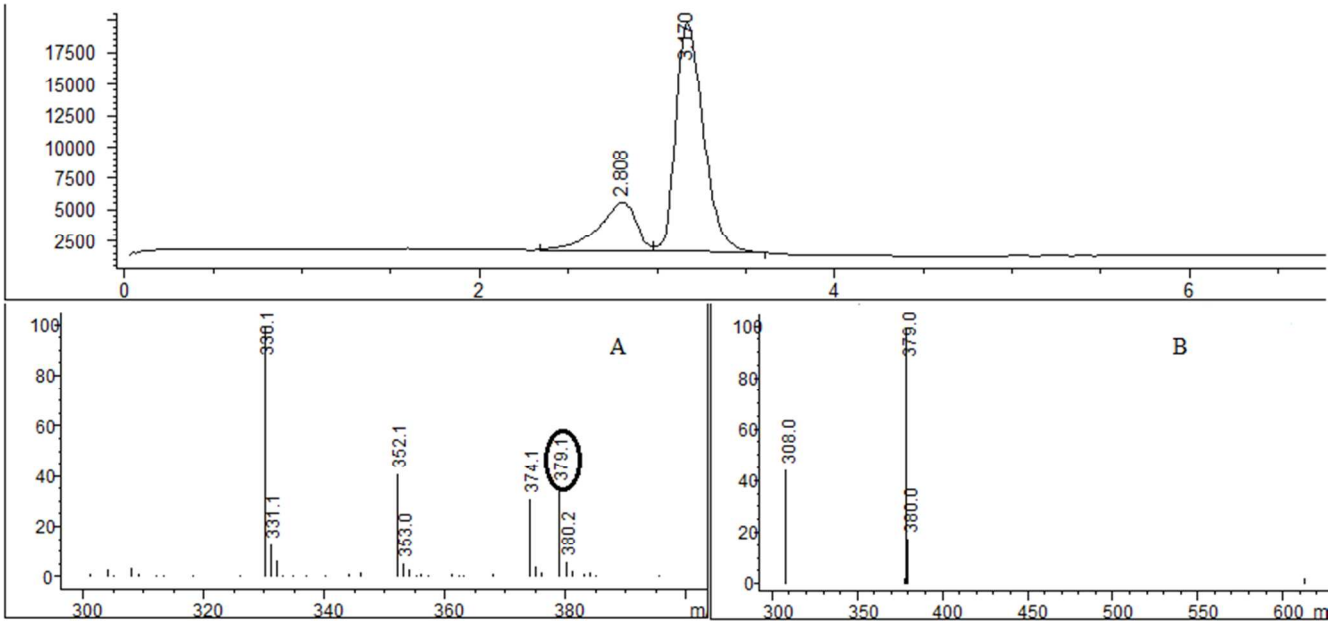

Figure 3: LC/MS Chromatogram, SIM, and scan spectra of a solution containing AA and GSH AA–SG complex (3.170 min); unreacted GSH (2.808 min). **A** and **B** are the scan and SIM mass spectra, respectively of AA–SG. The highlighted ion represents the protonated molecular ion, $[AA–SG + H]^+$

Variation of pH and Temperature

A plot of k_{obs} vs $[H^+]$ showing pH dependency for GSH at 310 K is shown in **Figure 4**. The model (line) shows excellent correlation to the experimental data indicating that the model fits the proposed mechanism depicted in equations (1) and (2). The second-order rate constant (k) and pK_s are calculated from this plot.

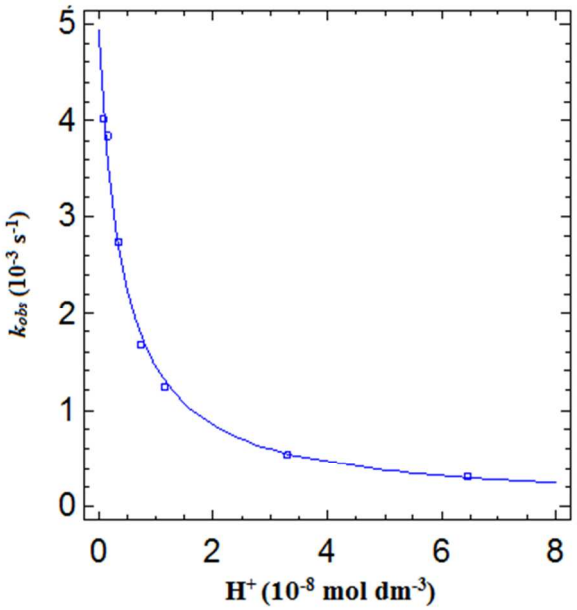

Figure 4: Plot of k_{obs} versus $[H^+]$ for GSH; Temperature 310 K; [AA] = 1.993 x 10^{-2} mol dm^{-3}

Reactions of *L*-Cysteine

Reaction of *L*-Cysteine and Ellman's Reagent in Tris/HCl Buffer

The repetitive-scan spectra and time traces (inset) for the reaction between CySH and ESSE are shown in **Figure 5**. The absorbance vs wavelength plot shows a clearly defined isosbestic point at 360 nm. The time trace shows that maximum absorbance of ES^- occurred after 30 seconds. This was maintained up to 600 seconds and gradually decreased thereafter; the reverse was true for the ESSE species. It was observed that the yellow solution (denoting the presence of $ES^–$) became colourless with time. Like GSH and other thiols, CySH forms the thiolate anion, $CyS^–$ in basic media. The $CyS^–$ ion is very reactive. It was suspected that $CyS^–$ was being quickly oxidized in the presence of oxygen in air to form the disulphide CyS–SCy, cystine, and $ES^–$ was reverting to ESSE.

Cite this: DOI: 10.1039/c0xx00000x

www.rsc.org/xxxxxx

FULL PAPER

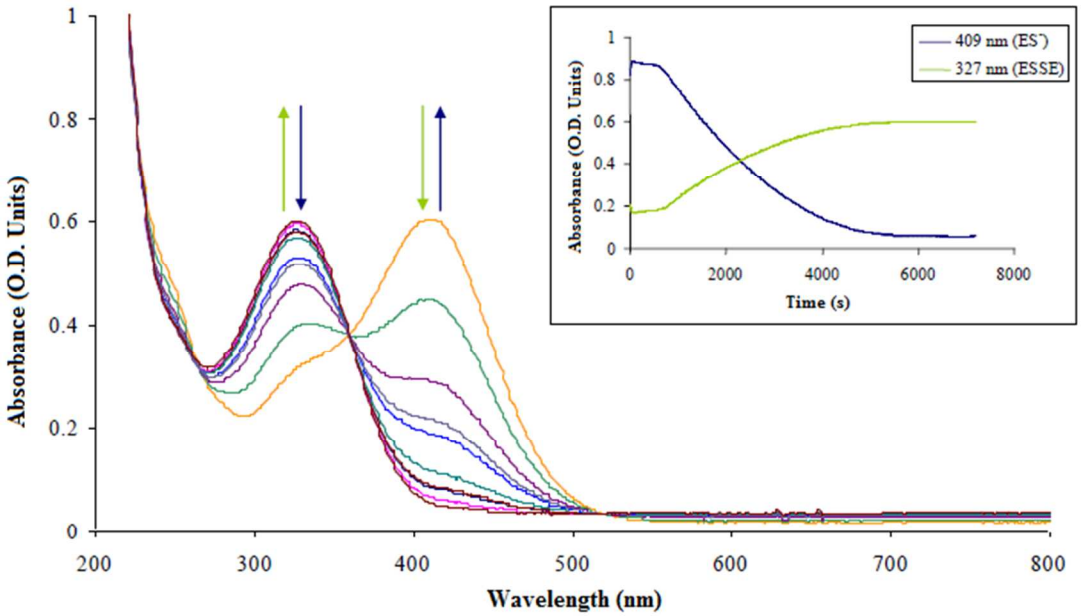

Figure 5: Repetitive-scan spectra of the reaction between ESSE and CySH (Inset: Absorbance-time trace showing the rates of appearance and disappearance of the ES^- and ESSE species. (blue arrows: initial reaction; green arrows: final reaction)

Reaction of *L*-Cysteine and Acrylamide

Like GSH, the reaction of CySH with a constant large excess of AA with varying [CySH] gives unchanged pseudo-first order rate constants, and increased linearly with an increase in $[AA]_T$, i.e. the reaction is pseudo-first order with respect to AA. Unlike GSH however, the plot does not pass through the origin; suggesting the occurrence of a reaction that is independent of the reaction between CySH and AA (**Figure 6**). A modified rate constant, k_{obs}, accounts for the non-zero intercept in equation (6) to give equation (9):

$$k_{obs} = \frac{kK_S[AA]}{K_S + [H^+]} + k_o \qquad (9)$$

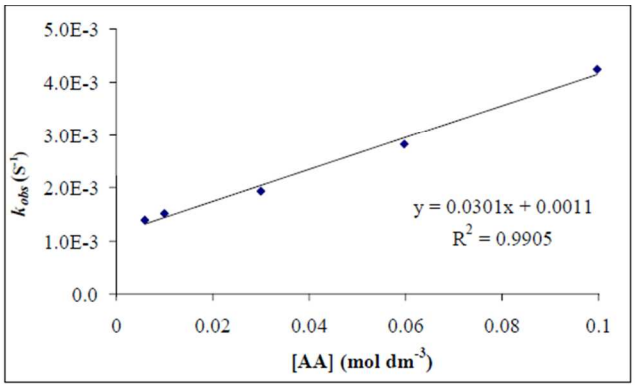

Figure 6: Pseudo-first order rate constants for the reaction of the thiol group of CySH with varying AA at 310 K; pH 7.4; [CySH] = 6.5 x 10^{-5} mol dm^{-3}

It is proposed that this independent reaction was the competitive oxidation of CySH by oxygen in air to form the disulphide, CyS–SCy, where k_o is the calculated rate constant for the oxidation of CySH by oxygen in air at 310 K. This independent reaction was investigated by adding a ten times excess of the known anti-oxidant, ascorbic acid (H_2Asc), to a reaction flask containing CySH. This inhibited the oxidation of CySH to the disulphide by reacting with the oxygen in air thus allowing CySH to react with AA.

This reaction mixture containing CySH and H_2Asc was reacted with ESSE as described in **Preliminary Studies**. It was observed that the reaction was stabilized by the presence of H_2Asc (evident by the yellow colour of the solution at the end of the reaction time of 9000 s, indicative of the presence of ES^-). This indicated that H_2Asc prevented the one electron oxidation of CySH as reported in a previous study conducted by Ohno et al. [28] As a result, 1.0 x 10^{-3} mol dm^{-3} H_2Asc was subsequently added to all CySH stock solutions prior to reaction with AA.

Equation (10) shows the reduction of cystine (CyS–SCy), the disulphide, to two molecules of cysteine. The oxidation of the other thiols by oxygen is slow in comparison to their reaction with AA and as a result no H_2Asc was added to those solutions.

$$CyS–SCy + 2e^- + 2H^+ \rightleftharpoons 2CySH \qquad (10)$$

Summary of Kinetic Results

Calculated second order rate constants, pK_s, and activation parameters for the reaction between AA with CySH, GSH, and CapSH are shown in **Table 3**.

Table 3: Summary of experimental results: Calculated second-order rate constants (k), activation parameters ($\Delta H^{\ddagger}$ $\Delta G^{\ddagger}$ $\Delta S^{\ddagger}$), and pK_s for the reactions between AA and RSH

Parameter	CapSH	CySH	GSH
k (dm^3 mol^{-1} s^{-1}) (293 K)	-	0.21 ± 0.01	-
k (dm^3 mol^{-1} s^{-1}) (298 K)	-	0.27 ± 0.02	-
k (dm^3 mol^{-1} s^{-1}) (303 K)	0.13 ± 0.01	0.34 ± 0.02	0.18 ± 0.02
k (dm^3 mol^{-1} s^{-1}) (310 K)	0.163 ± 0.003	-	0.25 ± 0.01
k (dm^3 mol^{-1} s^{-1}) (315 K)	0.19 ± 0.01	-	0.31 ± 0.04
Average pK_s	9.01 ± 0.05	7.4 ± 0.2	8.5 ± 0.2
Literature pK_s (298 K)	9.8 [b]	8.15 [a]	8.56 [a]
$\Delta H^{\ddagger}$ (kJ mol^{-1})	22 ± 7	34 ± 5	33 ± 5
$\Delta S^{\ddagger}$ (J K^{-1} mol^{-1})	-190 ± 2	-143 ± 2	-149 ± 2
$\Delta G^{\ddagger}$ (kJ mol^{-1}) (298 K)	78 ± 3	76 ± 1	78 ± 1

[a]ref 29; [b]ref 16

The pseudo-first order rate constants of the reaction between AA and the thiols: CapSH, CySH and GSH are greatly affected by pH in a manner that depends on the speciation of each thiol in solution. As pH increases, the thiol group becomes progressively more ionized, resulting in a higher concentration of the thiolate anion. The increase in k_{obs} values with increasing pH, for all three thiols, indicates that the thiolate anion is more reactive than the thiol.

The smaller rate constant obtained for CapSH's reaction with AA (compared to CySH and GSH) may be due to differences in minimized geometry (vide infra), acidity, hydrogen bonding, and solvent interactions at any stage of the reaction. The reported pK_s for CySH is 8.15 [29] while the experimental value is 7.4 ± 0.2 which is at the lower range of the buffer system that was used. The pK_s for GSH and CapSH are progressively larger (8.56 [29] and 9.8 [16] respectively), while our experimentally calculated values are: 8.5 ± 0.2 and 9.01 ± 0.05 for GSH and CapSH, respectively. The pK_s represents the pH at which there are equal amounts of RSH and RS$^-$. This implies that at the buffer range used (7.10 – 9.10 for Tris/HCl), a larger amount of CyS$^-$ is present in solution in comparison to GS$^-$ or CapS$^-$. This may explain why the reaction between AA and the three thiols has apparent order CySH > GSH > CapSH as indicated by k_{obs} at 303 K (**Table 1**). Although pK_s is temperature dependent, the measured values in our studies were unaffected by small variations in temperature. For all thiols, the experimentally derived entropies of activation ($\Delta S^{\ddagger}$) were negative, as may be expected for an associative mechanism in the transition state of the Michael-type addition mechanism. The experimental $\Delta S^{\ddagger}$ for the addition reactions was in the order: CapSH < GSH ~ CySH which can be attributed to significant intramolecular H-bonding in GSH stabilising the AA–SG transition state. Given that values of k for GSH are smaller than for CySH, a small steric effect on the Michael addition reaction is also possible. Furthermore, the possibility of intra-molecular H-bonding would make the S$^-$ less nucleophilic in GSH than CySH but not as significant as CapSH. We have investigated these possibilities with *ab initio* methods as presented in the next section.

Calculated Transition State Geometries and Reaction Path Energies

Figure 7 shows the calculated lowest energy conformations in the transition states (TS) that occur for CapSH, CySH and GSH in the gas phase. Similar structures are obtained when the optimization includes the effect of solvent water molecules (COSMO), except for CySH, where O6-H13 (intra-molecular) and H13-O24 (inter-molecular) distances (**Table 4**; *h*, *i* respectively) exceed that of typical medium strength H-bonds [30]. This likely arises from rotation of the terminal carboxyl group to maximize electrostatic interactions with the polar solvent. Otherwise, the number of significant O••HX contacts is unchanged by solvent, so that only water-phase predicted geometries (within the polarized continuum model) are discussed further below.

Table 4: Measurements (Å/deg) in calculated TS structures for CapSH, CySH and GSH

Measure	label	CapSH-AA		CySH-AA		GSH-AA	
		gas	water	gas	water	gas	water
S(11)-C(9)	*a*	2.355	2.515	2.299	2.499	1.995	1.938
S(11)-H(12)	*b*	1.650	1.730	1.616	1.728	1.490	1.495
H(12)-C(7)	*c*	1.482	1.389	1.539	1.402	1.822	1.812
C(9)-C(7)	*d*	1.427	1.417	1.433	1.417	1.468	1.486
C(7)-C(5)	*e*	1.477	1.487	1.469	1.485	1.432	1.422
C(5)-O(6)	*f*	1.240	1.248	1.248	1.251	1.281	1.286
C(5)-N(1)	*g*	1.383	1.362	1.381	1.361	1.370	1.385
O••HX	*h*	2.527	2.785	2.201	2.470	2.034	2.123
	i	4.021	4.056	2.412	2.883	2.048	2.066
	j			2.473	2.664	1.755	1.788
	k			3.048	2.657	1.837	1.880
	l					1.712	1.627
∠ S12-C9-H10	*m*	97.67	93.88	95.78	92.65	104.61	105.63

Cite this: DOI: 10.1039/c0xx00000x

www.rsc.org/xxxxxx

FULL PAPER

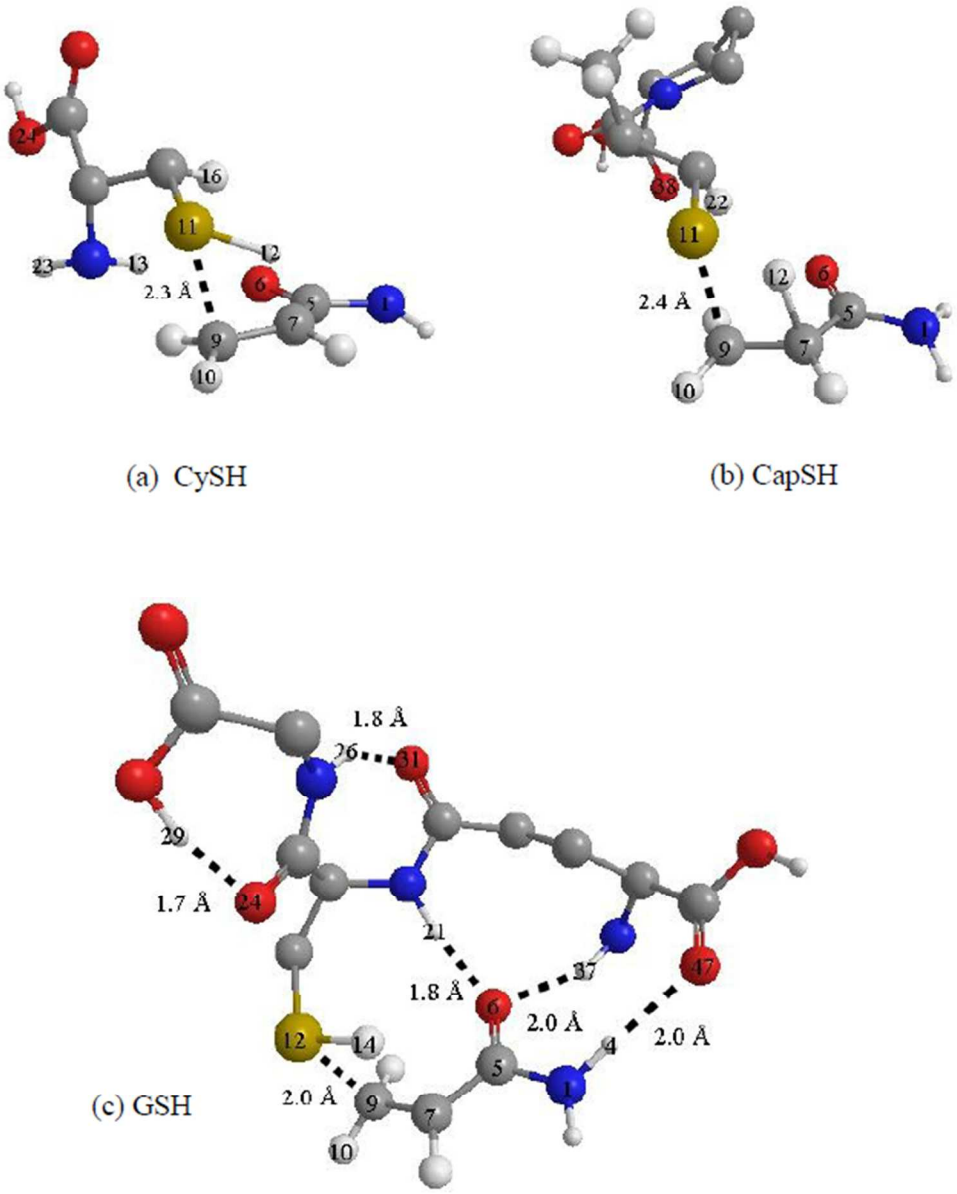

Figure 7: Perspective views of computed transition state structures for (a) CySH, (b) CapSH and (c) GSH reaction with acrylamide (non-essential hydrogens omitted).

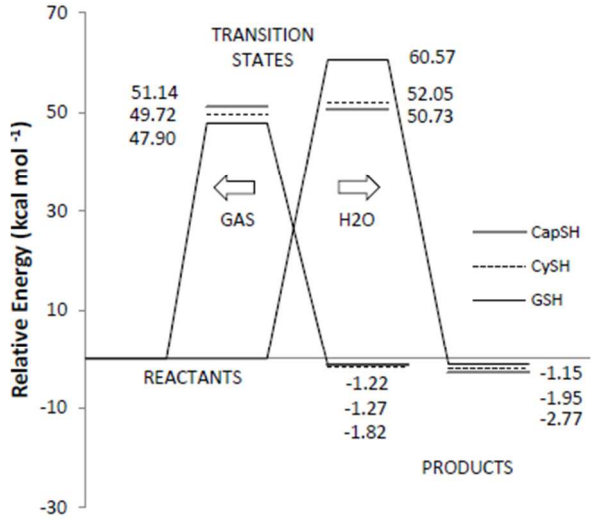

Figure 8: Theoretical minimum energy barriers for the reaction of CySH, CapSH and GSH with acrylamide in the gas phase and aqueous solution (DFT BVP86/TZVP/COSMO)

The gas phase energy barrier calculated for TS formation with AA and GSH (**Figure 8,** left) is lowest for the thiols studied, consistent with the intra-molecular H-bond contacts that are present in GSH but absent from the others. However, the net relative stabilization of the TS is only ~3.2 kcal mol^{-1} compared to the most energetic activation path shown by CapSH, suggesting that the positive entropy change which accompanies the formation of the TS is large enough to oppose the stabilizing enthalpic effect of the many intra-molecular H-bonds typical for many systems that have been studied in literature [30, 31]. The role of entropic contributions to the free energy changes is investigated in more detail below.

The solution phase energetics (**Figure 8,** right) are obtained from the gas phase data using the Hess's analysis shown in **Figure 9** and summarized in equations (11) and (12);

Table 5: DFT-computed thermodynamic parameters for the reaction of CapSH, CySH, and GSH with acrylamide at 298.15 and 303.15 K.

	$\Delta G^{\ddagger}$ (kcal mol^{-1})		$\Delta H^{\ddagger}$ (kcal mol^{-1})		$\Delta S^{\ddagger}$ (cal K^{-1} mol^{-1})		ΔG^{React} (kcal mol^{-1})		Equilibrium Constant	
Temp (K)	298.15	303.15	298.15	303.15	298.15	303.15	298.15	303.15	298.15	303.15
$CapSH_{(g)}$	51.14	51.38	36.77	36.76	-48.20	-48.22	-1.27	-1.03	8.52	5.54
$CapSH_{(aq)}$	50.73	50.90	38.42	38.35	-41.27	-41.40	-2.77	-2.61	107.82	76.56
$CySH_{(g)}$	49.72	49.94	36.33	36.34	-44.89	-44.88	-1.82	-1.62	21.75	14.70
$CySH_{(aq)}$	52.05	52.17	41.86	41.77	-34.18	-34.31	-1.95	-1.72	27.05	17.39
$GSH_{(g)}$	47.90	48.18	31.27	31.27	-55.77	-55.78	-1.22	-1.07	7.90	5.88
$GSH_{(aq)}$	60.57	60.56	52.58	52.29	-26.81	-27.28	-1.15	-0.90	6.93	4.45
	ΔG_{solv} (kcal mol^{-1})		ΔH_{solv} (kcal mol^{-1})		ΔS_{solv} (cal K^{-1} mol^{-1})		H-Bonding (kcal mol^{-1})		Activity Coefficient	
Acrylamide	-12.80	-12.57	-19.49	-19.14	-22.45	-22.03	-10.09	-9.76	2.45	2.49
CapSH (Prod)	-31.50	-31.08	-43.99	-43.26	-41.89	-40.86	-18.78	-18.16	6.89	7.51
CapSH (React)	-17.20	-16.93	-25.38	-24.91	-27.45	-26.76	-9.29	-8.98	61.44	64.46
CapSH (TS)	-30.41	-29.98	-43.22	-42.50	-42.98	-41.98	-18.92	-18.29	13.32	14.20
CySH (Prod)	-25.94	-25.50	-39.28	-38.58	-44.72	-43.86	-21.53	-20.81	4.86	4.76
CySH (React)	-13.02	-12.83	-18.87	-18.53	-19.64	-19.14	-8.01	-7.71	8.11	8.11
CySH (TS)	-23.48	-23.17	-32.84	-32.29	-31.38	-30.60	-16.64	-16.06	15.24	14.77
GSH (Prod)	-45.24	-44.47	-68.29	-67.09	-77.32	-75.85	-34.59	-33.44	1.85	1.97
GSH (React)	-32.52	-32.07	-46.22	-45.42	-45.94	-44.79	-21.98	-21.24	9.19	9.47
GSH (TS)	-32.64	-32.25	-44.40	-43.68	-39.44	-38.32	-16.13	-15.56	25.55	27.31

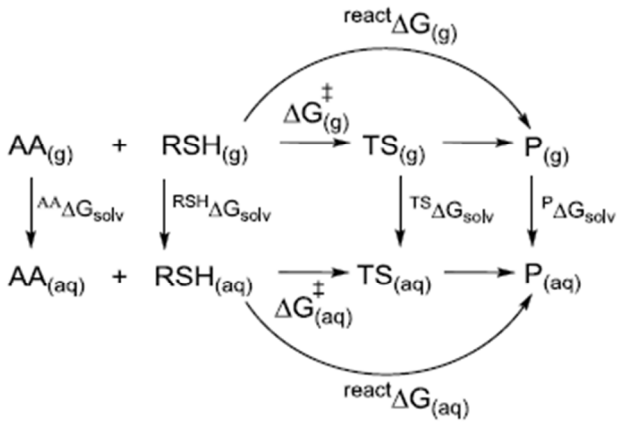

Figure 9: Thermodynamic scheme for free energy changes in gas phase and solution

$$\Delta G_{aq}^{\ddagger} = \Delta G_{g}^{\ddagger} + {}^{TS}\Delta G_{solv} - {}^{AA}\Delta G_{solv} - {}^{RSH}\Delta G_{solv} \qquad (11)$$

$${}^{React}\Delta G_{aq} = {}^{React}\Delta G_{g} + {}^{P}\Delta G_{solv} - {}^{AA}\Delta G_{solv} - {}^{RSH}\Delta G_{solv} \qquad (12)$$

where AA = acrylamide, RSH = thiol, TS = transition state, P = product and $\Delta G^{\ddagger}$ is the activation free energy change in gas phase or aqueous medium.

Following gas phase *ab-initio* calculations, the free energy of solvation at infinite dilution, H-bond interaction energy, and the activity coefficient for each component in water were calculated with the COSMO-RS module of the ADF software. By assuming that the heat capacity of each molecule is constant over a small temperature range [32], the slope of the free energy of solvation with temperature affords an estimate of the enthalpic and entropic contributions to the total free energy change of solvation [33]. We use a ±30 K margin at 6 K intervals around 298.15 and 303.15 K to determine the relevant entropic terms in each case. Gas phase free energies are also corrected by degrees of freedom component analysis at each specified temperature. **Table 5** presents the

combined thermodynamic results.

The differences in activation free energy for CapSH, CySH and GSH at 298 K when the effects of solvation are included in the computation (**Figure 8**, right), are -0.41, +1.33 and +12.7 kcal mol^{-1} respectively. The small decrease for CapSH and slight increase for CySH are unlikely to be significant given the intrinsic limitations of each step in the computation, but the TS of GSH is predicted to be significantly less accessible in water. If dissociation of the thiol is a necessary first step in the reaction mechanism, then a polar solvent such as water will stabilize the charged reactant species and hence increase the energy of activation as observed in **Figure 8**.

According to the experimental acid dissociation constants (**Table 3**), GSH is more easily dissociated than CapSH, so its stabilization by water should be larger. For theoretical comparison, we compute the Hirshfeld charges on the reactive functionality, C-SH, as an estimate of nucleophilicity in the minimum energy conformations obtained in gas and aqueous phase (**Table 6**).

Table 6: Atomic Hirshfeld Charges in Gas Phase and Aqueous Solution[c]

	C		S		H	
	(g)	(aq)	(g)	(aq)	(g)	(aq)
CapSH	-0.069	-0.069	-0.035	-0.037	0.044	0.044
CapSH†	-0.070	-0.075	0.026	-0.036	0.048	0.045
CySH	-0.076	-0.075	-0.056	-0.058	0.032	0.032
CySH†	-0.074	-0.079	0.036	-0.050	0.050	0.048
GSH	-0.073	-0.078	-0.017	-0.018	0.045	0.040
GSH†	-0.056	-0.054	0.206	0.221	0.060	0.058

[c] †Transition State

In both gas and solution, the computed sequence of estimated nucleophilicity of the sulphur atom in the thiol is CySH > CapSH > GSH, where CapSH and GSH are reordered compared to experiment. Coupled with the reordering in reaction rates, this finding suggests that the extent of formation of the thiolate anion is variable and is not only dependent on pK_s and that solvent and hydrogen bonding interactions may be important. In particular, inter- and intra-molecular hydrogen bonding that stabilize a gaseous transition state are likely to be disrupted by water molecules in solution, adding to the relative increase in activation energy. On inspecting the derived enthalpy ($\Delta H^{\ddagger}$) and entropy ($\Delta S^{\ddagger}$) contributions to $\Delta G^{\ddagger}$ for GSH (**Table 5**), we note the reaction in aqueous solution gives the smallest change in $\Delta S^{\ddagger}$ and the largest change in $\Delta H^{\ddagger}$ of the thiols studied. This pattern is a complete reversal of the findings for the gas phase reaction, supporting the effect of H-bond interactions on the activation energy in solution; the highest free energy change with solvation (ΔG_{solv}) for the AA product, reactant and transition states all occur in the reaction of GSH. We may also assign the reversal of activation energies for CySH and CapSH in water as being due to the combination of limited H-bonding capability of CapSH and its large p*Ks* (9.0 experimental), but the computed difference is small at 1.32 kcal mol^{-1}.

The computed free energy of reaction (ΔG_{React}) for all three thiols with acrylamide are also small, the largest at -1.82 kcal mol^{-1} for CapSH. However, the small differences between thiols are expected to have significant impact on the thermodynamic equilibrium constants computed in each case according to:

$$K_{eq} = \exp\left(\frac{-\Delta G^{React}}{RT}\right) \quad (13)$$

We obtain values of 108, 27 and 7 mol L^{-1} for CapSH, CySH, and GSH, respectively at 298 K (**Table 5**). There are several transition state models which seek to relate, with varying degrees of success, theoretical activation parameters to experimentally derived rate constants [34-36]. Our computed kinetic values of rate constants, k_s, activation free energy, $\Delta G^{\ddagger}_{s}$ and Arrhenius pre-factor A_s (s for *in silico*) are shown in **Table 7**.

Table 7: Experimental and theoretical estimates of rate constants, *k*, Arrhenius pre-factor, A and activation parameters ($\Delta G^{\ddagger}$, $\Delta H^{\ddagger}$, and $\Delta S^{\ddagger}$) for the reaction of AA with CapSH, CySH and GSH[d]

	$\Delta^o G^{\ddagger}$	$\Delta^o H^{\ddagger}$	$\Delta^o S^{\ddagger}$	rate constant (dm^3 mol^{-1} s^{-1})		Arrhenius	
	(kcal mol^{-1})	(kcal mol^{-1})	(cal mol^{-1} K^{-1})	*k*	k_s	ln A	ln A_s
CapSH	18.64	5.26	-45.41	0.13	1.28E-24	7.93	9.64
CySH	18.16	8.13	-34.18	0.34	1.55E-25	13.04	13.21
GSH	18.64	7.89	-35.61	0.18	1.38E-31	12.58	16.74

[d] s for *in silico*

There is marked disparity between the experimental and theoretical kinetic parameters in **Table 7**, but relatively good agreement is obtained for the standard entropy change of activation with all three thiols (-41.3, -34.2, -26.8 cal mol^{-1} K^{-1}) for CapSH, CySH and GSH from theory, **Table 5**). Closely matching the kinetic variables with experimental data for these reactants in aqueous solution will likely require higher level DFT computational methods with the Moller-Plessett Perturbation Theory [37] (MP2), larger basis sets, Variational Transition-State Theory [32] (VTST) and isotopic labelling experiments since the transition state involves a proton migration. However, given that AA may react ~500 times faster with -SH than with -NH_2 that are both present in biologically active thiols [10, 38] our results have established that dominant reaction between AA and thiols is probably the Michael addition between the more nucleophilic -S^- groups and AA. In particular, a linear isokinetic plot of $\Delta H^{\ddagger}$ versus $\Delta S^{\ddagger}$ for the reactions described above (a correlation coefficient > 0.99) gave an isokinetic temperature of 260 ± 24 K and an intercept value for $\Delta G^{\ddagger}$ of 71 ± 4 kJ mol^{-1} (17 ± 1 kcal mol^{-1}, **Figure 10**). Although there is controversy in literature about the nature of enthalpy-entropy compensation (whether it is real [39-41] or artefact [42, 43]) most workers support its existence. The isokinetic temperature represents the temperature at which the rates of reaction between AA and all three thiols are equal. The presence of a linear isokinetic plot for RSHs confirms that the reactions between AA and all three thiols follow a similar general reaction mechanism i.e. the Michael addition.

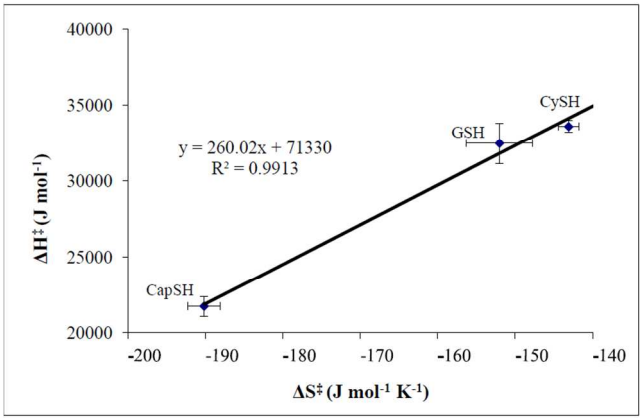

Figure 10: Isokinetic plot for the reactions between AA and the thiols – CapSH, CySH and GSH

Conclusions

Thiols are known to react with acrylamide, a potential carcinogen, formed in carbohydrate food preparations above 100 °C. In this paper, we report the kinetics of the reaction of acrylamide with three common thiols, CapSH, CySH and GSH according to a Michael addition reaction scheme. Assuming that the nucleophilicity of all three thiols is approximately the same, the rates of the reaction with AA were expected to follow: CySH > CapSH > GSH, reflecting the increasing molecular size of the thiols. However this was not observed. Rather, the experimental reaction rate follows the order CySH > GSH > CapSH. DFT calculations support the experimental results through marked effects of solvation and hydrogen bonding on the activation energies, where the GSH–AA activated complex is computed at 8-10 kcal mol^{-1} higher than CapSH and CySH. This is consistent with diminished *intra*-molecular hydrogen bonding in GSH–AA due to more *inter*-molecular interactions with the polar water solvent molecules. We obtained an experimental linear entropic-enthalpy compensation plot from $\Delta G^{\ddagger}$, $\Delta H^{\ddagger}$, $\Delta S^{\ddagger}$, activation parameters which support a single pathway for all three thiols. Recent reports [32] suggest that the calculation of rate constants could be bettered using Variational Transition State Theory with MP2 correlation, or with explicit treatment of the role of water molecules (ex Solvent Assisted Proton Exchange or SAPE models [44, 45]) which we expect to form part of our future work.

Notes

a Department of Chemistry, The University of the West Indies, St. Augustine, Trinidad and Tobago, W.I. Fax: 1868-645-3771; Tel:1868-662-6013 E-mail: grace-anne.bent@sta.uwi.edu; richard.fairman@sta.uwi.edu; lebert.gierson@sta.uwi.edu*

b Department of Chemistry, The University of the West Indies, Mona, Kingston 7, Jamaica, W. I. Fax: 1876-977-1835; Tel:1876-927-1910; E-mail: paul.maragh@uwimona.edu.jm; tara.dasgupta@gmail.com

† Electronic Supplementary Information (ESI) available: [details of any supplementary information available should be included here]. See DOI: 10.1039/b000000x/

‡ This work was supported by funding provided by the Office of Graduate Studies and Research, The University of the West Indies, Mona, Jamaica, West Indies and the Departments of Chemistry, The University of the West Indies, Mona, Jamaica and St. Augustine, Trinidad and Tobago.

References

1. I.A.R.C., I.A.R.C. Monogr. Eval. Carcinog. Risks Hum., 1994, **60**, 389 - 433.
2. I.A.R.C., I.A.R.C. Monogr. Eval. Carcinog. Risks Hum. , 1986, **39**, 403.
3. I.A.R.C., I.A.R.C. Monogr. Eval. Carcinog. Risks Hum. Suppl. 7, 1987, 56.
4. , 2003.
5. E. Tareke, P. Rydberg, P. Karlsson, M. Törnqvist and S. Eriksson, Chem. Res. Toxicol., 2000, **13**, 517 - 522.
6. G.-A. Bent, P. Maragh and T. Dasgupta, Food Chem. , 2012, **133**, 451-457.
7. E. Tareke, P. Rydberg, P. Karlsson and M. Törnqvist, J. Agric. Food Chem., 2002, **50**, 4998 - 5006.
8. K. Galesa, U. Bren, A. Kranjc and J. Mavri, J. Agric. Food Chem., 2008, **56**, 8720-8727.
9. G. Tong, W. Cornwell and G. Means, Toxicol. Lett., 2004, **147**, 127 - 131.
10. M. Friedman, J. Agric. Food Chem., 2003, **51**, 4504 - 4526.
11. J. Wilson, D. Wu, R. Motiu-Degrood and D. A. Hupe, J. Amer. Chem. Soc., 1980, **102**, 359 - 363.
12. K. Kolšek, M. Sollner Dolenc and J. Mavri, Chem. Res. Toxic., 2013, **26**, 106-111.
13. J. Mavri, Toxicol. In Vitro, 2013, **27**, 479-485.
14. A. Pastore, F. Piemonte, M. Locatelli, A. L. Lo Russo, L. M. Gaeta, G. Tozzi and G. Federici, Clinical Chem., 2003, **8**, 1467-1469.
15. J. Castell, M. Gomez-Lechon, X. Ponsoda and R. Bort, Arch. Toxicol., 1997, 313 - 321.
16. P. Ribeiro, A. Santini, H. Pezza and L. Pezza, Eclet. Quim., 2010, **35**, 179-188.
17. O. Pecháňova, Physiol. Res., 2007, **56** S41-S48.
18. C. Napoli, V. Sica, F. De Nigris, O. Pignalosa, M. Condorelli, L. Ignarro and A. Liguori, Am. Heart J., 2004, **148**, e5.
19. M. Harrison and M. Baldwin, Org. Mass Spectrosc., 1989, **24**, 689 - 693.
20. A. D. Becke, Phys Rev A, 1988, **38**, 3098-3100.
21. A. Schafer, H. Horn and R. Ahlrichs, J. Chem. Phys., 1992, **97**, 2571-2577.
22. J. Baker, T. Janowski, K. Wolinski and P. Pulay, WIREs Comput. Mol. Sci., 2012, **2**, 63-72.
23. A. Klamt, J. Phys. Chem., 1995, **99**, 2224-2235
24. A. Vrije Universiteit, The Netherlands.
25. C. C. Pye, T. Ziegler, E. van Lenthe and J. N. Louwen, Can. J. Chem., 2009, **87**, 790-797.
26. F. L. Hirshfeld, Theoretica Chimica Acta, 1977, **44**, 129.
27. K. B. Wiberg and P. R. Rablen, J. Comp. Chem. , 1993, **14**, 1504.
28. Y. Ohno, K. Ormstad, D. Ross and S. Orrenius, Toxicol Appl. Pharmacol., 1985, **78**, 169 - 179.
29. M. Friedman, J. Cavins and J. Wall, J. Amer. Chem. Soc. , 1965, **87**, 3672 - 3682.
30. G. A. Jeffrey and S. Takagi, Accounts of Chemical Research, 1978, **11**, 264-270.
31. C. L. Perrin and J. B. Nielson, Annu. Rev. Phys. Chem. , 1997, **48**, 511-544.
32. D. E. Smith and A. D. J. Haymet, J. Chem. Phys. , 1993, **98**, 6445-6454.
33. N. R. Syme, C. Dennis, A. Bronowska, G. C. Paesen and S. W. Homans, J. Am. Chem. Soc. , 2010, **132**, 8682-8689.
34. B. C. Garrett and D. G. Truhlar, Variational Transition State Theory, in Theory and Applications of Computational Chemistry: The First Forty Years, Elsevier B.V., 2005.
35. T. Bartsch, J. M. Moix, R. Hernandez, S. Kawai and T. Uzer, Adv. Chem. Phys., 2008, **140**, 191-238.
36. C. J. Cramer, Essentials of Computational Chemistry: Theories and Models, John Wiley and Sons Ltd., 2004.
37. C. Møller and M. S. Plesset, Phys. Rev., 1934, **46**, 618-622.
38. J. M. Rice, Mutat. Res., 2005, **580**, 3 - 20.
39. L. Liu and Q.-X. Guo, Chem Rev., 2001, **101**, 673-695
40. K. F. Freed, J. Phys. Chem B, 2001, **115**, 1689-1692.

41. J. F. Douglas, J. Dudowicz and K. F. Freed, Physical Review Letters, 2009, **103**, 135701-135704.
42. A. Cornish-Bowden, J. Biosci., 2002, **27**, 121 -126.
43. A. Cooper, C. M. Johnson, J. H. Lackey and M. Nollmann, Biophys. Chem. , 2001, **93**, 215-230.
44. C. A. Bayse, J. Phys. Chem B, 2007, **111**, 9070-9075.
45. C. A. Bayse, Org. Biomol. Chem., 2011, **9**, 4748.